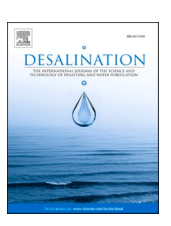
ELSEVIER

Contents lists available at ScienceDirect

Desalination

journal homepage: www.elsevier.com/locate/desal





Application of the radiotracer method to study the fouling of tubular microfiltration membranes

Agnieszka Miśkiewicz^{a,*}, Grażyna Zakrzewska-Kołtuniewicz^a, Jakub Iwanicki b

- a Institute of Nuclear Chemistry and Technology, Dorodna 16, 03-195 Warsaw, Poland
- ^b Faculty of Chemical and Process Engineering, Warsaw University of Technology, Warynskiego 1,00-645 Warsaw, Poland

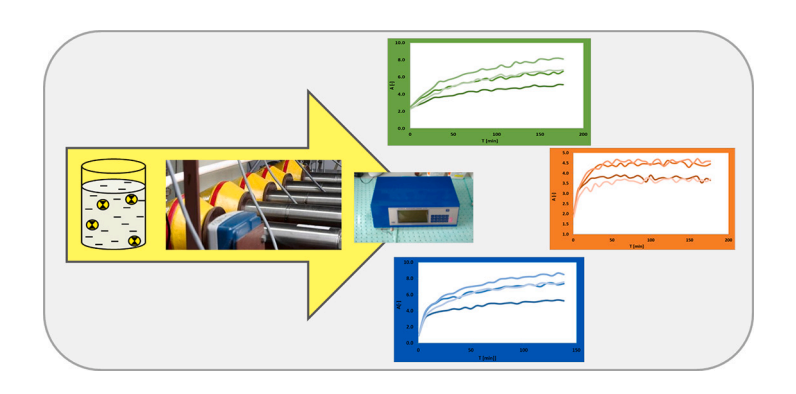
HIGHLIGHTS

- Fouling of membranes used for LRW treatment was studied by the radiotracer method
- The polyacrylic acid (PAA) with different MWs was used as a model fouling agent.
- The effect of MW of PAA on particles distribution along the membrane was examined
- The PAA molecules with the lowest MW blocked the membrane surface the fastest.
- Different mechanisms of fouling can occur depending on the MW of PAA.

ARTICLE INFO

Keywords: Microfiltration Liquid radioactive waste Membrane fouling Radiotracers

G R A P H I C A L A B S T R A C T



ABSTRACT

This paper presents a study on the fouling of ceramic microfiltration (MF) membrane. Such membranes are often used in the treatment of liquid radioactive waste. In the investigation of the phenomenon of fouling, a radiotracer method with a short-lived lanthanum isotope (140 La) is applied. The effect of the molecular weight (MW) of the complexing agent, used to bind the radionuclides in the MF-enhanced process, was studied in radiotracer experiments. Poly(acrylic acid) with a MW of 30 kDa, 100 kDa and 250 kDa is used as the complexing agent. The distribution of particles with different MWs at various positions along the membrane module is examined. The test results show that the particles with the lowest MW (i.e. 30 kDa) blocks the membranes the quickest, causing the greatest decrease in the permeate flux. However, the amount of deposit formed on the membrane, which is reflected by the level of radioactivity measured, is

Abbreviations: A, Absolute radioactivity (–); A_i , Radioactivity at a given time (cps - counts per second); A_o , Initial radioactivity (cps - counts per second); A_P , Radioactivity of the permeate (cps - counts per second); A_P , Radioactivity of the feed (cps - counts per second); A_P , Absolute radioactivity in the equilibrium state (–); E_1 , E_2 , E_3 , Energies of gamma rays (keV); E_D , Electrodialysis; k_P , Initial rate of the PAA deposition (min⁻¹); k_P , Permeate flux (l m⁻² h⁻¹); k_P , Flux of water (l m⁻² h⁻¹); k_P , Pseudo-first order rate constant (min⁻¹); k_P , Pseudo-second order rate constant (min⁻¹); k_P , Low-level radioactive waste; k_P , Membrane distillation; k_P , Microfiltration; k_P , Molecular weight (g mol⁻¹); k_P , Polyacrylic acid; k_P , Polymer-assisted ultrafiltration; k_P , Polyethyleneimine; k_P , Retention coefficient (%); k_P , Correlation coefficients (%); k_P , Reverse osmosis; k_P , Total organic carbon content (mg/l).

E-mail address: a.miskiewicz@ichtj.waw.pl (A. Miśkiewicz).

^{*} Corresponding author.

the lowest in this case. This indicates the existence of different membrane blocking mechanisms, which depend on the size of the particles contained in the filtered medium.

1. Introduction

Low-level radioactive waste (LLW) is generated by the use of radioactive substances in medicine, industry and science. The operation of nuclear installations also has a large share in the generation of radioactive waste [1]. Regardless of the reactor type liquid LLW is always produced during its operation, its conservation works or its decommissioning. Since liquid, low-level waste is usually very diluted, the risk to the environment is lower. However, it is still necessary to manage such waste by concentrating the radioactive components into a small volume and then, after the appropriate conditioning, to store them safely in a radioactive waste repository. However, recovered water can be reused or discharged into the environment. Among the methods that can be used to treat LLW, one should mention the membrane techniques [2-4]. Such methods have already been applied to liquid low-level radioactive waste processing, with new solutions under continuous research [5-11]. These include, above all, reverse osmosis (RO) [5,6] and other pressure methods [7-12], but also electrodialysis (ED) [13] and membrane distillation (MD) [14,15] processes are possible. Compared to other separation methods, membrane techniques have many advantages that make them attractive; these include a high decontamination factor, a relatively low energy consumption and a compatibility with existing systems. Despite these advantages, these methods do have some weaknesses and limitations. A major one is membrane fouling, which as a result limits the widespread use of membrane processes in industry. To minimize this unfavorable phenomenon, a variety of countermeasures are made. These methods include the initial purification of the feed, the appropriate design of membrane modules (e.g. the use of moving parts in the so-called dynamic filtration) [16,17] and the proper regulation of the process parameters (such as the critical flux or the use of a strong transverse flow) [18].

To more effectively counteract this fouling phenomenon, it is necessary to thoroughly understand its nature and its consequences via systematic scientific research. It has been reported in many papers that membrane fouling is determined by many factors, among others:

membrane properties (pore size, hydrophobicity, charge); foulant characteristics (molecule weight (MW), charge, hydrophobicity and composition) as well as hydrodynamic conditions (transmembrane pressure, cross-flow velocity) [19,20]. Studies on the particle size distribution showed that colloids and dissolved organic substances, which blocked membrane pores, formed a cake layer on the membrane surface, seriously reducing membrane permeability and contributing more to the fouling than particulates [21]. However, there are not many reports in the literature on the study of the distribution of particles of different sizes along tubular membrane modules.

Many methods have been tested and proposed for the analysis of membrane fouling over the years [22-27]. Each of these methods undoubtedly have its advantages and limitations. Hence, in practice, the appropriate method is selected for a specific application, which accounts for the membrane type, the module configuration, the properties of the filtered medium, etc. An interesting approach involves the study of fouling by use of radiotracers, i.e. radioactive substances in very low concentrations. The presence of these substances, and their movement inside membrane apparatuses, can be tracked by detecting the radiation that they emit. Radiotracer techniques are non-invasive and nondestructive methods that do not require the use of sophisticated equipment. They are well-developed methods that have been adopted for the study of many apparatuses operating in the chemical industry [28]. Therefore, these methods can act as an excellent tool for a study of the processes that occur within the membrane apparatus. The use of radiotracer methods for concentration polarization [29], as well as membrane fouling investigations [30,31], has been described in several previous works. These studies showed that it is a very promising method for a qualitative and qualitative description of the fouling phenomenon.

This paper presents, using a radiotracer method, an analysis on the fouling of a tubular ceramic microfiltration (MF) membrane. Ceramic membranes are resistant to harmful influences, including ionizing radiation, and can be used, for example, at the preliminary treatment stage of liquid radioactive waste. This preliminary stage is necessary to minimize the fouling of the membranes used in further stages that involve the processing of waste (e.g. RO membranes) and to extend their

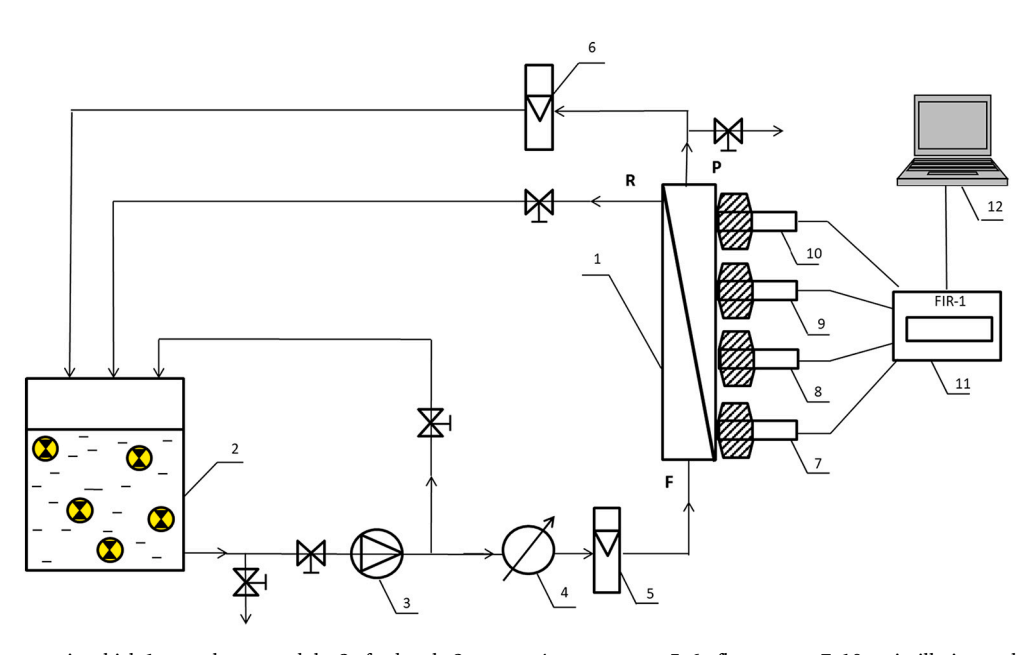


Fig. 1. Experimental set-up, in which 1 - membrane module, 2 - feed tank, 3 - pump, 4 - manometer, 5, 6 - flowmeters, 7–10 - scintillation probes, 11 - radiometer, 12 - PC.

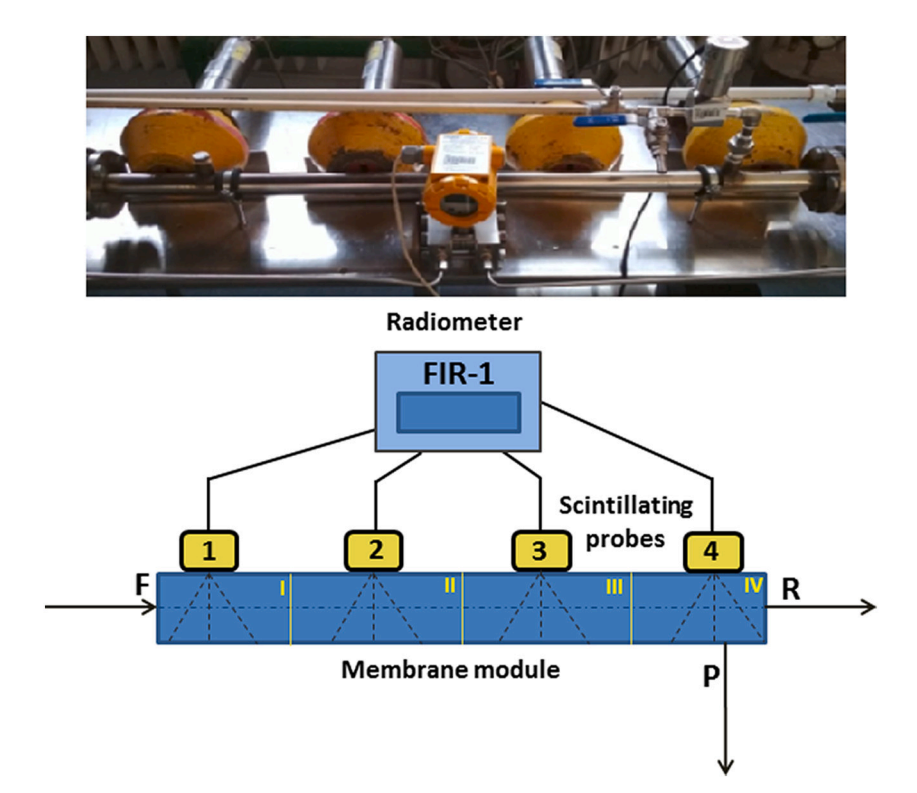


Fig. 2. The arrangement of the scintillating probes (1–4), positioned along the membrane module, and the schematic division of the membrane module into 4 sectors (I - IV).

lifetime. However, if the membranes are used in a pretreatment step, they may be exposed to blockage since liquid radioactive waste often contains some solid materials as well as soluble macromolecular compounds that may deposit on the surface of the membranes and/or penetrate into their pores. One of the macromolecular compounds, which can be used for complexation of radionuclides during the processing of radioactive waste, are chelating water-soluble polymers such as polyacrylic acid (PAA) and its soluble salts or polyethyleneimine (PEI). These macromolecular compounds are used in polymer-assisted PAUF for liquid radioactive waste treatment and can be present in wastewater [32]. The PAA has been selected as a model substance that causes membrane fouling in the experiments described in this work. In particular, this paper presents studies on the effect of the molecular weight of poly(acrylic acid) on the deposit formation on the tubular membrane as well as the distribution of this deposit along the membrane. A radiotracer method, using one of the lanthanum isotopes ¹⁴⁰La, was applied. This radionuclide was chosen due to its short half-life ($au_{1/2}$ = 1.678 days) as well and high energy of gamma rays it emits (E_1 = 487.0, $E_2 = 815.77$ and $E_3 = 1596.21$ keV), moreover, due to the effective attachment of its cationic form (140La³⁺) to PAA molecules.

2. Materials and methods

2.1. Chemicals

All the chemicals used in this work were of analytical grade purity. Poly(acrylic acid) with a molecular weight of 100 and 250 kDa (Sigma Aldrich) and 30 kDa (Plyscience Inc.) were employed. Lanthanum nitrate (La(NO $_3$) $_3$ ·6H $_2$ O) was purchased from BDH Chemicals. Sodium hydroxide and citric acid were obtained from CHEMPUR, Poland, and the nitric acid was from POCH, Poland. Distilled water was used in all experiments.

2.2. Experimental set-up

An installation, equipped with a membrane module, operating in a cross-flow regime was used; the representative diagram of which is shown in Fig. 1. A ceramic tubular membrane, 0.1 μm pore size (1), most often used at INCT for the treatment of the institutional radioactive wastewater, were selected for the research. The membrane was made of Al_2O_3 and it was provided by Atech Innovations, GmbH. The filtration area of the membrane was 0.05 m^2 , internal diameter - 16 mm and a length - 1 m.

The experiment was set-up as follows: the feed solution (F) was taken from the feed tank (2) by means of a screw pump (3) (type AFJ 20.1 B, JOHSTADT), and it was then directed to the membrane module. The retentate (R) and permeate (P) streams were returned to the feed tank (2), so that the installation operated in a closed circuit. The system was also equipped with control and measurement devices, such as a manometer (4) (type EN 837-1, Aplisens) and two flow meters: one measures the feed flow (5) (type UMF2-B11F0BH0, Heinrichs) and the other the permeate flow (6) (type DPM - 1507G2C334P, KOBOLD). There were also three valves; two valves were used to adjust the flow rate of the feed solution and third one was a reducing valve that regulates the pressure in the system. Four scintillation probes in the lead collimators (6-10) were positioned along the membrane module (1). The probes were connected to the industrial FIR-1 (INCT, Poland) radiometer (11). The arrangement of probes along the membrane module is shown in Fig. 2.

The arrangement of scintillation probes, along the membrane module, was chosen in a way that enabled a division of the module into 4 sectors (I - IV). Readings from probe No. 1, in particular the increase in recorded radioactivity, measured the development of a PAA layer in the inlet part of the membrane module (sector I). Probes No. 2 and No. 3 recorded the PAA behavior in the middle part of the module; namely in sectors II and III, respectively. The last probe, No. 4, was located closest to the permeate outlet and it was responsible for recording the radioactivity in sector IV of the membrane.

Table 1Testing the durability of radiotracer binding.

Polymer	Initial radioactivity [cps]	1st cycle of washing		2nd cycle of washing		3rd cycle of washing	
		A [cps]	% of leaching	A [cps]	% of leaching	A [cps]	% of leaching
PAA 30 kDa	24.00	0.80	3.33	0.35	1.47	0.18	0.76
PAA 100 kDa PAA 250 kDa	18.56 19.33	0.00 0.00	0.00 0.00	0.00 0.00	0.00 0.00	0.00 0.00	0.00 0.00

Table 2Retention coefficient of PAA determined by two method: by measuring the radioactivity and TOC of the samples.

Polymer	R (by measuring radioactivity)	TOC [mg/l]		R (by measuring TOC)
	[%]	Feed	Permeate	[%]
PAA 30 kDa	$84.34 \pm 5\%$	61.29	5.86	$90.44\pm1.6\%$
PAA 100 kDa	$100.00\pm5\%$	60.42	4.78	$92.09 \pm 1.2\%$
PAA 250 kDa	$100.00\pm5\%$	52.72	2.13	$95.97\pm0.4\%$

3. Experimental

3.1. Preparation of the radiotracer

To prepare the solution that feeds through the membrane installation, poly(acrylic acid) radiolabeled with radioactive ¹⁴⁰La, which was initially a sample of nonradioactive La(NO₃)₃ with a mass of 60 mg, was exposed to a neutron stream at 5×10^{13} neutrons s⁻¹ m⁻² in the Maria reactor (National Center for Nuclear Research, Świerk, Poland). The sample was irradiated for 1 h and then cooled for 12 h. The radiotracer had an initial activity of approximately 5 MBq. Next, 140 La(NO $_3$) $_3$ was dissolved in 1 cm³ of 1 M HNO₃. The resulting solution was used as the radiolabeling material. Then, 3 dm³ of 0.1 g dm⁻³ polyacrylic acid solution was prepared, to which 0.9 g of La(NO₃)₃•6H₂O was added as the non-active carrier for the radiotracer. Subsequently, around 20–250 \times 10⁻⁶ dm³ of the radiotracer was added dropwise to the polyacrylic acid solution. After mixing the reagents, the pH of the solution was adjusted to a value of 5 by adding the appropriate amounts of HCl and NaOH, both with a concentration of 1 M. To allow the radiotracer to react with the polyacrylic acid (PAA), the solution was stirred using a magnetic stirrer for 2 h. Three separate solutions were prepared: PAA with molecular mass 30 kDa, 100 kDa and 250 kDa. Each solution, in separate experiments, would then act as the feed for the membrane installation (Fig. 1).

3.2. Radiotracer stability testing

Before starting the studies of the tubular ceramic membrane with the use of 140 La as a radiotracer, as usual, the stability of its binding to PAA molecules was checked. For this purpose, for each PAA with a molecular weight of 30, 100 and 250 kDa the following experiment was performed:

To the lanthanum nitrate (non-active carrier for the radiotracer) with the concentration of La(III) equal to 0.1 g/L the polyacrylic acid solution was added. Subsequently, small portion of radiotracer was added dropwise to the solution. After the reagents are mixed, the pH of the solution was adjusted to a value of 5 by adding the appropriate amounts of HCl and NaOH, both with a concentration of 1 M. To allow the radiotracer to react with the polyacrylic acid, the solution was stirred using a magnetic stirrer for 2 h. After this time, the reaction mixture was filtered using flat-sheet membrane made of PES with MW cut-off of 5 kDa (Merck-Millipore) in an Amicon 8400 stirred membrane cell

(Merck-Millipore) to separate the phases, i.e. the radiolabeled PAA molecules, from the solution containing any unbound radiotracers ions. Then the residue in the membrane cell was washed with 3 portions of water and filtered using the same membrane as before (PES, 5 kDa). During the washing, the radioactivity of the washing solution was measured. In the case of PAA with MW 100 and 250 kDa, zero activity of the solution was recorded (Table 1), which indicates a complete lack of elution of the radiotracer from the labeled phase, which means that it is permanently bound. In the case of PAA with MW of 30 kDa, a slight leaching of the radiotracer was observed, ranging from 0.8–3.3%.

In the case of this MW (30 kDa), an incomplete retention of the polymer- 140 La complex on the membrane was also observed, as evidenced by about 80% retention of 140 La (Table 2). This was confirmed by the determination of the PAA concentration in the feed as well as in the permeate streams by measuring the Total Organic Carbon (TOC) content (using TOC analyzer Multi C/N 3100, Analityk Jena) of samples collected from those streams Therefore, probably the radioactivity of the washing solution observed during stability studies may result from the further passage of the labeled polymer through the membrane, and does not mean that the radiotracer is bound unstably.

3.3. Filtration of PAA solutions labeled with ¹⁴⁰La

The initial stage, before the start of each experiment, involved cleaning the membrane system and then measuring the flux of the distilled water, J_w . The water flux, determined before each experiment, was $192 \pm 5 \text{ dm}^3 \text{ m}^{-2} \text{ h}^{-1}$. Afterwards the feed tank was filled with the feed solution, which was a PAA solution with a specific MW (i.e. 30, 100 or 250 kDa) labeled with radioactive lanthanum (prepared as described in Section 3.1). Filtration was performed under a constant pressure of 10⁵ Pa and a constant flow rate of 200 dm³ h⁻¹ for the feed solution. During the experiments, both the permeate flux, J_{ν} , and the level of its radioactivity, A_P , were examined. The permeate flux was determined by means of a measuring cylinder, while the level of radioactivity of the permeate samples was measured using a gamma counter (LG-1b type, INCT, Poland). At the beginning of the experiments, permeate samples were collected every 15 min and then, after one hour, every 30 min. During the filtration of the radiolabeled PAA solution, the radioactivity of the deposit that accumulated on the membrane surface (or inside its pores) was continuously measured. This measurement was made via the four scintillation probes that are arranged along the membrane module, as shown in Fig. 2. After the experiment was completed, the system was first rinsed with citric acid or sodium hydroxide solutions of 1% concentration. Then, in order to wash out the acid and base residues, the installation was rinsed with distilled water until the feed solution conductivity was equal to that of pure water.

4. Results and discussion

The lanthanum radiotracer enabled the ability to track the changes in the amount of PAA deposited onto the tubular membrane, in each of its individual sectors, during the filtration of the PAA solution. The results of the study of the deposit distribution for PAA with different MWs (i.e. 30, 100 and 250 kDa) are presented below. The kinetics of the blocking of the membrane in each of the sectors, which are found to depend on

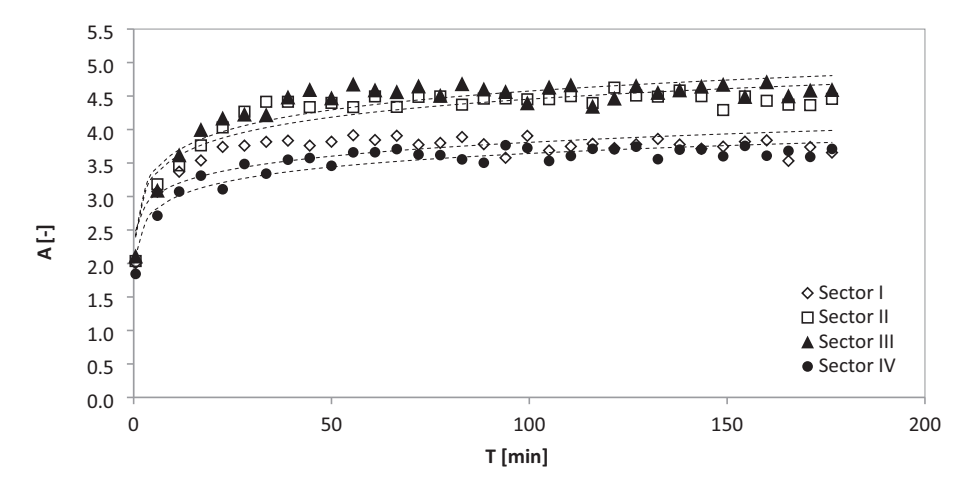


Fig. 3. Time dependence of the absolute radioactivity for PAA with a molecular weight 30 kDa.

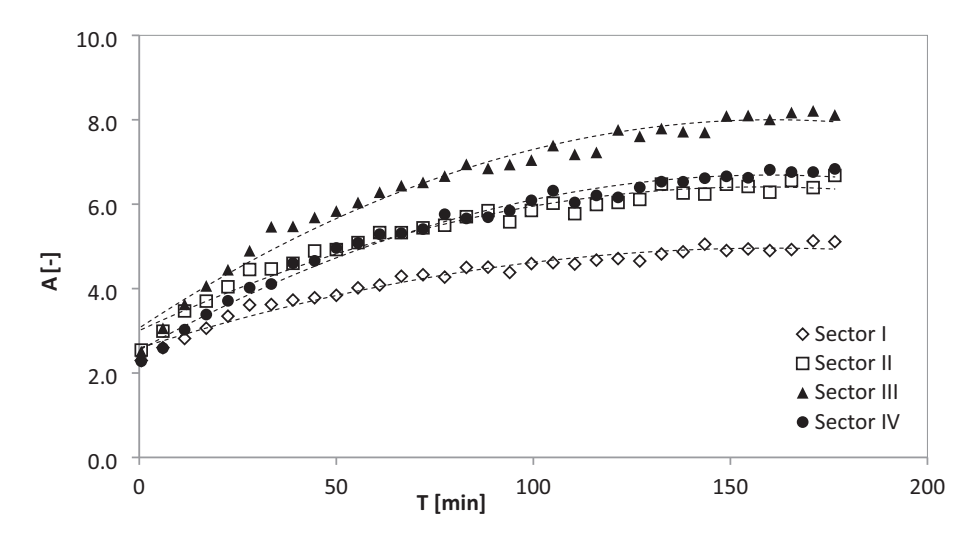
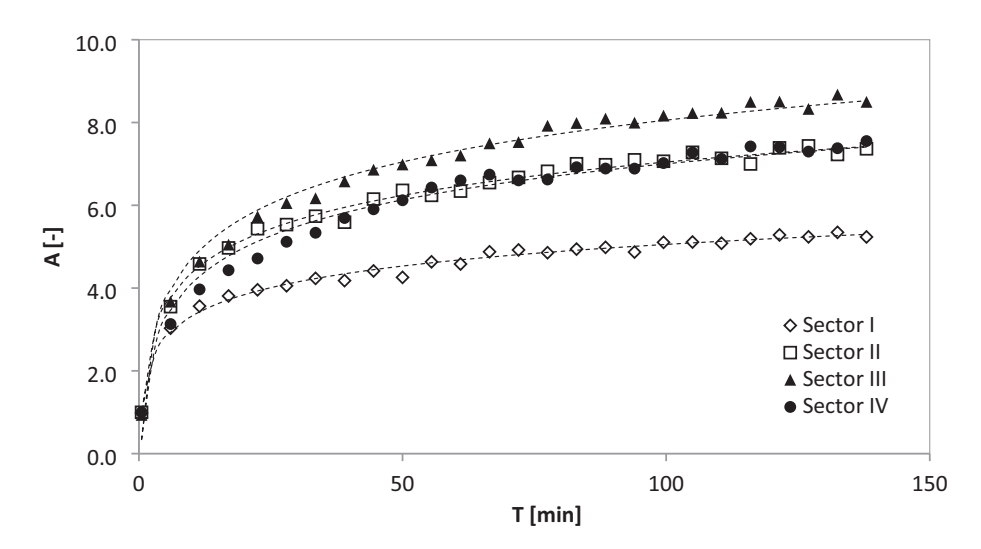


Fig. 4. Time dependence of the absolute radioactivity for PAA with a molecular weight 100 kDa.



 $\textbf{Fig. 5.} \ \ \text{Time dependence of the absolute radioactivity for PAA with a molecular weight 250 kDa.}$

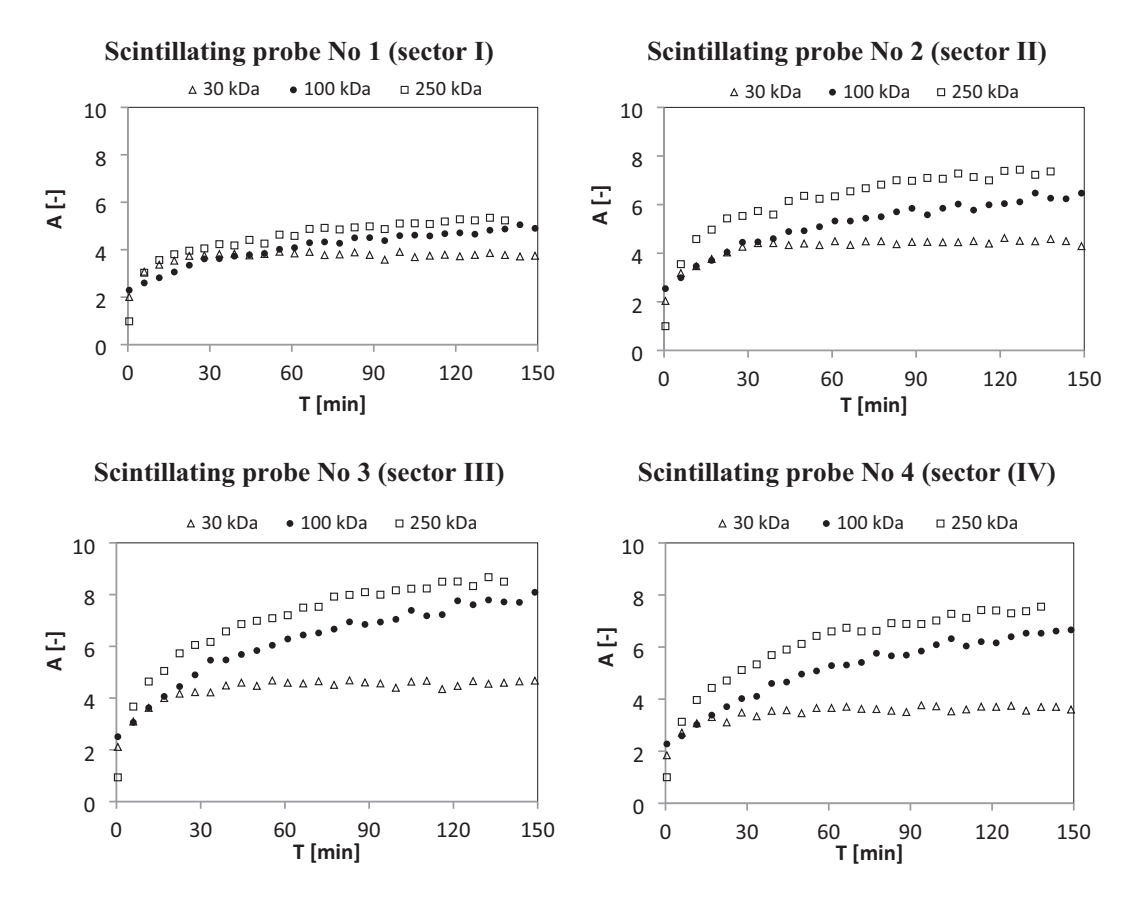


Fig. 6. Absolute radioactivity versus time for the four scintillation probes (membrane sectors).

the MW of the PAA, are also analyzed.

4.1. Distribution of the deposit dependent on the molecular weight of the PAA

The experiments consisted of the measurement of the radioactivity of the radioabeled PAA, which accumulated on the membrane module in its four sectors (I-IV). An increase in the radioactivity indicates a gradual build-up of the PAA layer on the membrane surface, as well as its accumulation in the membrane pores. To accurately present the results of the measurements, an absolute radioactivity value, A, is used. Absolute radioactivity is defined as the ratio of the radioactivity at a given time, A_i , recorded by the scintillation probe (in cps, counts per seconds) to the initial radioactivity, A_0 , of the stock solution, which is also determined by scintillation probe, i.e.:

$$A = \frac{A_i}{A_0}. (1)$$

The time dependence of the absolute radioactivity for PAA with different molecular weights (i.e. 30, 100 and 250 kDa), which is accumulated in the individual membrane sectors during the filtration process, are shown in Figs. 3–5.

The increase in the absolute radioactivity, as shown in Fig. 3, proves that the deposit layer grows during the filtration. Differences in the absolute radioactivity, for individual scintillating probes positioned in different sectors of the membrane module, indicate a non-uniform accumulation of the deposit along the length of the tubular membrane. The largest increase in radioactivity recorded from the precipitate, thus also - as can be expected - the greatest layer thickness, was recorded for probes No. 2 and No. 3. These are located in the middle of the module (sectors II and III, respectively) and their absolute radioactivity values are comparable. In contrast, smaller values were obtained

for probes No. 1 (sector I) and No. 4 (sector IV). The low A value for probe No. 1 results from the increased flow turbulence at the inlet of the membrane, which is caused by inlet mixing effects that reduce deposit formation. Downstream of the membrane module, the flow was established, the turbulence was reduced and, therefore, the fouling was increased. The lowest absolute radioactivity value was recorded at the exit of the system – namely, for probe No. 4 located in sector IV, which is positioned downstream of the permeate outlet port. Here, a direction change of the solution flow and a mixing zone with increased turbulence were created, which meant that the molecules had difficultly settling on the surface of the membrane or accumulating in the pores of the membrane. Previous studies on the hydrodynamics of the flow in the tested module (Fig. 1) showed the existence of a different types of flow along this module [31]. These earlier radiotracer investigations have revealed that, in the first zone of the module, the turbulent flow is generated because of the feed stream entering the module. In the other zones of the module, the flow stabilizes and a flow close to the plug flow is formed.

Additionally, current research has shown that the value of the absolute radioactivity stabilizes quite quickly during the filtration process using PAA with MW of 30 kDa, and an equilibrium state is achieved after approximately 1 h. The same stabilization occurs in all the sectors of the membrane module (Fig. 3).

Analyzing the graph that depicts the change in the absolute radioactivity during filtration of PAA with a MW of 100 kDa (Fig. 4), a quite fast increase in the absolute radioactivity during the process can be observed. Thus, we can conclude that the deposit layer increases on the surface of the membrane. The lowest value of *A* was obtained for the scintillation probe located at the inlet of the module (sector I). This can be explained in a similar manner to the 30 kDa PAA filtration case, in that the turbulence increase in the inlet zone reduces the fouling. The flow stabilizes and the turbulence decreases along the membrane, which makes it easier for the sediment to accumulate on the membrane surface;

Table 3Absolute radioactivity of the deposit accumulated in the different sectors of the membrane module, which are obtained for PAA with different molecular sizes.

MW of PAA	A [-]					
	Sector I	Sector II	Sector III	Sector IV		
30 kDa	3.75	4.52	4.56	3.61		
100 kDa	4.93	6.56	8.18	6.87		
250 kDa	5.34	7.31	8.69	7.55		

this is reflected by the measurements from probes No. 2 and No. 3 (sectors II and III, respectively). The highest absolute radioactivity values were obtained from probe No. 3 measurements. This probe was positioned farther away from the inlet of the membrane module compared to probe No. 2, for which the flow is less turbulent and, thus, there is a more intense accumulation of PAA molecules on the surface of the membrane than anywhere else. The values of A obtained in sector IV confirms the effects of the permeate outlet on diminishing the fouling in this sector. As in the case of filtration of PAA with 30 kDa (Fig. 3), the absolute radioactivity decreases close to the outlet of the module, due to the increased turbulence for the flow that is caused, in turn, by the change in the direction of the solution flow. However, the decrease in the A value in sector IV for PAA with 100 kDa was unable to achieve the same A values obtained in sector I (which was the case when PAA with 30 kDa was filtrated, see Fig. 3). Moreover, in the case of PAA with 100 kDa, a visible increase in the value of A in sector III compared to sector II was observed. Such relationships were not observed for PAA with 30 kDa, for which A values for these two sectors (i.e. II and III) were almost identical. When comparing PAA with the two molecular masses 30 and 100 kDa, the difference in behavior can be explained by the smaller susceptibility of the higher mass to changes in the flow structure and the greater ability to deposit on the membrane.

Results obtained for PAA with 250 kDa (Fig. 5) are similar to those obtained for PAA with 100 kDa. In these cases, the lowest values of the absolute radioactivity are observed in sector I and the highest arise in sector III of the membrane module.

Graphs showing the accumulation of PAA (with different molecular weights) on the membrane in the individual module sectors are presented in Fig. 6. Moreover, for a clearer comparison of the obtained results, the values of the absolute radioactivity, *A*, in individual sectors for different MW of PAA, which are obtained at the end of the process, were compared and presented in Table 3.

Based on Fig. 6 and Table 3, it can be concluded that the smallest

difference in the absolute radioactivity, depending on the MW of the filtered particles, is visible in sector I. A greater difference appears in sector II, but the greatest variation can be observed in sectors III and IV. In the case of particles with a MW of 100 and 250 kDa, the A values are similar in each of the sectors; although a slightly higher value of A is obtained for 250 kDa. In contrast, the absolute radioactivity obtained for PAA with 30 kDa significantly differs to the others, namely it is significantly lower than the value of A obtained during the filtration of particles with higher molecular weights (i.e. 100 and 250 kDa). This relationship is visible for each of the four sectors of the membrane module.

These dependences can be explained by analyzing the changes in the retention of PAA over time for all the considered MWs. To determine the efficiency of the separation of the polymer particles, measurements of the radioactivity of the collected permeate samples were performed. Assuming that 140 La is permanently bound to the PAA molecule, we can conclude that by measuring the radioactivity of the permeate, P, and the feed solution, F, an actual measure of the radioactivity of the radiolabeled PAA particles present in these streams is obtained. Therefore, the retention coefficient, R, of PAA can be calculated from the following expression:

$$R = 1 - \frac{A_P}{A_F},\tag{2}$$

where A_P and A_F represent the radioactivity deriving from the radiolabeled particles of PAA in the permeate and the feed, respectively, in units of cps.

The change in the retention coefficient over time for the three different masses of PAA is presented in Fig. 7.

Particles with the smallest MW (i.e. 30 kDa) largely pass through the membrane, which is proven by the significant decrease in R from 78% to 41%. Hence, this may result in the lowest radioactivity of the deposit recorded in radiometric tests for PAA molecules of this mass compared to the radioactivity obtained in studies with larger PAA particles (Fig. 6 and Table 1). Some of the particles that accumulate on the membrane may also enter its pores, thus blocking them and reducing the permeate flux. This possibility was confirmed by the measurements of J_v , the results of which are presented in Fig. 8. For the larger MWs of PAA (i.e. 100 and 250 kDa), the decrease in R was not that significant, which indicates that the larger particles were better retained by the membrane. For both these MWs, after the initial decrease in R, its gradual increase was observed over the duration of the filtration. This may indicate the creation of a so-called "secondary membrane", which is formed by the

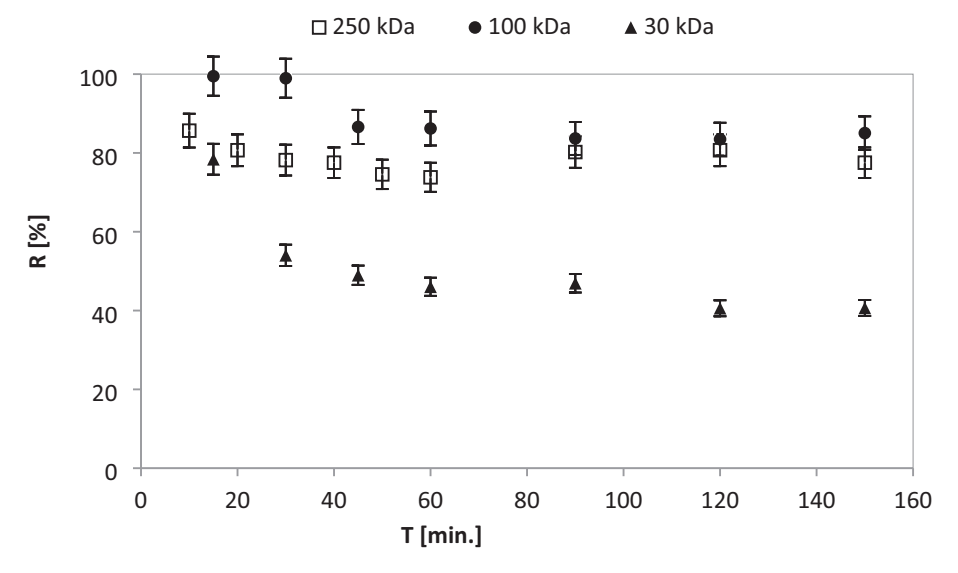


Fig. 7. The change in the retention coefficient, R, during the filtration of PAA with different MWs.

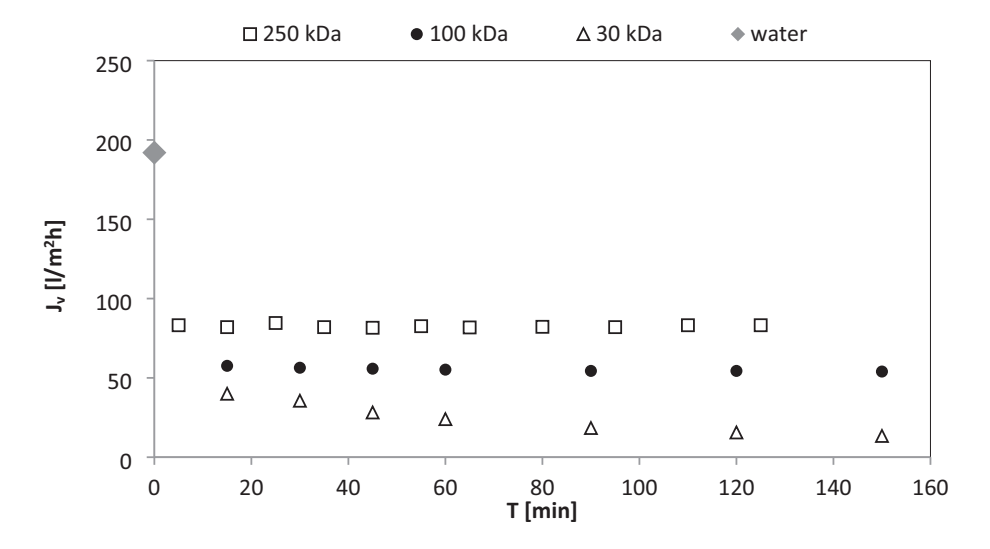


Fig. 8. The change in the permeate flux, J_{ν} , during the filtration of PAA with different MWs.



Fig. 9. A simplified diagram of the differences in the deposit layer structure depending on the particle size, assuming the sphericality of the foulant particles.

deposited layer, that enhances the separation capacity of the membrane. Additionally, it should be noted, as seen in Fig. 7, that the largest R factors were obtained for 100 kDa. This indicates a more complicated nature of the separation with the hybrid method and confirms the large influence of membrane fouling on the separation effect. In contrast to the permeate flux, which declines with formation of the polymer layer, the retention factor may improve due to the formation of the secondary membrane. The secondary membrane may have different properties depending on the molecular size of the complexing agent. It can be denser for smaller particles and more, loose for larger complexes (Fig. 9).

A dense membrane increases retention rates more than a porous one. This is the case with the experiment with 100 kDa and 250 kDa polymers, which is indicated by an increase in R coefficients after a temporary decrease related to the stabilization of the process conditions. Moreover, the R factors for the membrane-PAA 250 kDa system are not evidently the highest. It seems that the effect of the denser secondary membrane formed by the 100 kD PAA is greater and decisive than that of the more loose secondary membrane formed by the 250 kD PAA.

When 30 kDa PAA is used, retention is mainly influenced by the membrane, the pores of which are too large to trap small complexes, and the secondary membrane, as shown in tracer studies, is very thin.

By analyzing the variation of J_{ν} over time, a rapid decline in the permeate flux for all the studied PAAs can be observed at the beginning of the process (Fig. 8). It then stabilizes with the highest J_{ν} value that can be achieved being observed for PAA with 250 kDa. Particles with higher MW, such as 250 kDa, probably create a more porous cake on the membrane surface compared to particles with lower MW (i.e. 100 or 30 kDa), which allows a greater sized permeate flux. The experiments with the smallest PAA particles (i.e. 30 kDa), showed the lowest value of J_{ν} as well as the greatest decrease for this parameter during the filtration

process. Due to their small size, the particles can penetrate deeper into the pores of the membrane, accumulate there and effectively block them.

It should be noted that the above observations and discussion on membrane blocking mechanism concern the specific case of the membrane we use, i.e. the membrane with pore size relatively larger than the size of the foulant particles.

4.2. Kinetic studies

Pseudo-first-order and pseudo-second-order models were employed to investigate the kinetics of the deposition of the PAA with different molecular weights. During the attempt to describe the fouling of the tested membrane, other kinetic models were also taken into account. However, it was assumed that a model describing the obtained results, on the one hand, should precisely describe them, but on the other hand it should be as simple as possible. Typically to describe the rate of the adsorption of particles on the membrane surface these two models are considered [33–35].

The equation representing the pseudo-first-order model is given by:

$$\frac{dA_t}{dt} = k_1(A_e - A_t) \tag{3}$$

which can be rearranged to provide a linearized data plot, alongside an integration over the boundary conditions t=0 to t=t and $A_t=0$ to $A_t=A_b$ so that:

$$log(A_e - A_t) = logA_e - k_1 \times t/2.303 \tag{4}$$

where A_t is the absolute radioactivity at time t (in minutes), A_e is the absolute radioactivity in the equilibrium state and k_1 is the pseudo-first-

Table 4Constants relevant to the applied kinetic models for the deposition rate of PAA.

	Membrane sector	I	II	III	IV
	Pseudo-first-order				
30 kDa	A _{e, exp} [-]	3.7	4.5	4.6	3.7
	k ₁ [1/min]	0.7402	0.9129	0.9048	0.7920
	A _{e, cal} [-]	21.1	29.7	31.5	18.8
	$R^{2}[-]$	0.8882	0.8090	0.7789	0.805
100 kDa	$A_{e, exp}[-]$	5.1	6.7	8.1	6.8
	k ₁ [1/min]	0.7957	0.9670	1.2192	1.120
	A _{e, cal} [-]	28.3	49.3	75.1	49.4
	$R^2[-]$	0.3491	0.3793	0.3824	0.334
250 kDa	$A_{e, exp}[-]$	5.2	7.4	8.5	7.5
	k ₁ [1/min]	1.8507	2.2171	2.4442	2.204
	A _{e, cal} [-]	35.2	73.7	96.9	69.5
	$R^2[-]$	0.8795	0.8715	0.8412	0.794
	Pseudo-second-order				
30 kDa	$A_{e, exp}[-]$	3.7	4.5	4.6	3.7
	k ₂ [1/min]	0.3828	0.1644	0.1198	0.129
	A _{e, cal} [-]	3.7	4.5	4.6	3.7
	$R^{2}[-]$	0.9975	0.9986	0.9983	0.998
100 kDa	$A_{e, exp}[-]$	5.1	6.7	8.1	6.8
	k ₂ [1/min]	0.0246	0.0095	0.0063	0.007
	A _{e, cal} [-]	5.3	7.0	8.9	7.5
	$R^2[-]$	0.9932	0.9916	0.9886	0.989
250 kDa	$A_{e, exp}[-]$	5.2	7.4	8.5	7.5
	k ₂ [1/min]	0.0225	0.0137	0.0094	0.010
	A _{e, cal} [-]	5.5	7.8	9.3	8.1
	R^2 [-]	0.9955	0.9958	0.995	0.994

order rate constant of the PAA deposition on the membrane (in units of inverse minutes).

The pseudo-second-order model is expressed by:

$$\frac{dA_t}{dt} = k_2(A_e - A_t)^2 \tag{5}$$

Separating the variables of which gives:

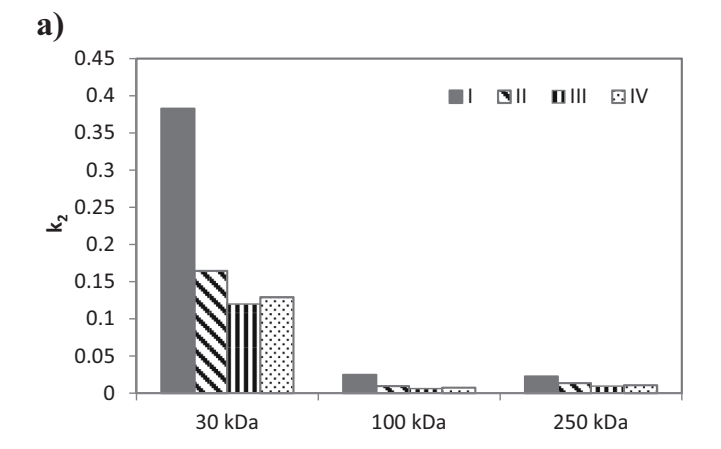
$$\frac{dA_t}{\left(A_e - A_t\right)^2} = k_2 dt \tag{6}$$

By integrating this expression, with the boundary conditions and a rearrangement, we obtain:

$$\frac{t}{A_t} = \frac{1}{h} + t / A_e \tag{7}$$

$$h = k_2 A_e^2 \tag{8}$$

where h is the initial rate of the PAA deposition (at t=0), and k_2 is the pseudo-second-order rate constant of the PAA deposition on the membrane (1/mins).



To evaluate how consistent the experimental data is with the kinetic models, the correlation coefficients R^2 , kinetic rate constants, and the experimental and calculated values of the absolute radioactivity were analyzed (Table 4).

The correlation coefficients for the linear plots, from the pseudosecond-order rate model, are greater than 0.995 in all the membrane sectors (with exception of PAA with 100 kDa, in which R^2 is about 0.99). This suggests that the PAA deposition on the membrane is consistent with the pseudo-second order model. The comparison of the two parameters, i.e. k_2 and A_e , cal, obtained from the kinetic calculations for this model (in which PAA has different MWs) and the four membrane sectors is shown in Fig. 10(a) and (b), respectively. When considering the PAA deposition rate, represented by the constant k_2 , it can be observed that the highest values of this parameter were obtained for PAA with 30 kDa (Fig. 10(a)). This rather fast deposition for 30 kDa PAA in all the membrane sectors and the obtained equilibrium of the deposition are shown in Fig. 3. This can be explained by the decrease seen in the retention coefficient of the 30 kDa particles (Fig. 7) and, thus, the decrease in the amount of particles in the feed solution. As shown in Fig. 10(b), the lowest values of A_e for all the membrane sectors were achieved for these particles. However, this does not modify the fact that these small sized PAA molecules (compared to the other particles under consideration) contributed to the greatest decrease in the permeate flux (Fig. 8). This proves that a different pattern arises for membrane blocking by particles with 30 kDa compared to larger massed particles, as was discussed earlier (Section 4.1).

Additionally, a much higher rate for the deposition on the membrane is seen in the first zone of the membrane (sector I) when compared to other sectors, which is noticeable for PAA with all the considered MWs. In the first sector of the membrane module, i.e. at the inlet of the system, the flow is quite turbulent due to the insertion of the feeding solution. Therefore, in this enhanced mixing zone, the fast-flowing particles are not able to settle so readily, and the first layer that is formed does not grow as quickly over the duration of the filtration process.

5. Conclusion

This paper described a fouling analysis for a tubular ceramic MF membrane, which included the application of the radiotracer method. The suitability of the latter, which requires relatively simple equipment, was confirmed for the non-invasive and non-destructive testing of membrane fouling. The research included studies on the effects of different molecular weights of poly(acrylic acid) on the deposit formation, as well as the distribution of this deposit at various positions along the membrane module under examination. Based on the presented results, it was concluded that the PAA molecules were not evenly distributed along the membrane module, which was due to flow

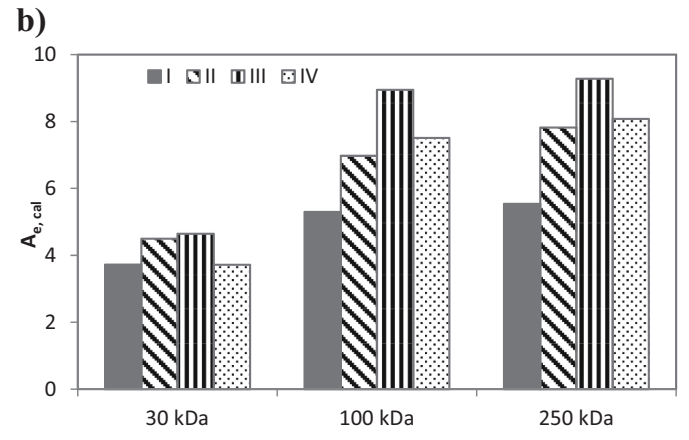


Fig. 10. Comparison of the kinetic parameters (a) k_2 and (b) A_e , which are obtained in different sectors of the membrane for PAA with different MWs.

disturbances in certain areas of the membrane (i.e. the inlet and outlet stream effects in sectors I and IV). Moreover, such a distribution is dependent on the molecular weight of the PAA. In addition, the conducted tests showed that the lowest mass PAA (at 30 kDa) blocks the membrane differently when compared to larger mass PAA, possibly due to its insertion into the pores of the membrane, which causes a significant decrease in the permeate flux. It should be emphasized that the above findings resulting from the conducted research concern the case of fouling of microfiltration tubular membranes with a pore size larger than the size of the substance causing this phenomenon.

Analysis of the kinetics of the PAA deposition on the tested membrane showed that it closely aligns with the pseudo-second-order model, which is indicated by the high correlation coefficients. The highest values of the rate constants, k_2 , were obtained for PAA molecules with the lowest molecular weight. Additionally, the rate constants are determined to be greatest in the first sector of the membrane module. It is hoped that the obtained results may contribute to an improved understanding of the phenomenon of fouling, which will be especially important for the nuclear industry, and thus it could aid the development of methods designed to reduce it.

CRediT authorship contribution statement

Agnieszka Miśkiewicz: Conceptualization, Methodology, Data curation, Writing- Original draft preparation, Visualization, Validation, Writing- Reviewing and Editing.

Grażyna Zakrzewska-Kołtuniewicz: Supervision, Writing-Reviewing and Editing.

Jakub Iwanicki: Investigation.

Declaration of competing interest

The authors declare that they have no known competing financial interests or personal relationships that could have appeared to influence the work reported in this paper.

Acknowledgments

This research was funded by the International Atomic Energy Agency for Coordinated Research Project on the Management of Wastes Containing Long lived Alpha Emitters (T13017).

References

- Classification of Radioactive Waste, General Safety Guide No. GSG-1, International Atomic Energy Agency, Vienna, 2009.
- [2] G. Zakrzewska-Trznadel, Advances in membrane technologies for the treatment of liquid radioactive waste, Desalination 321 (2013) 119–130, https://doi.org/ 10.1016/j.desal.2013.02.022.
- [3] G. Zakrzewska-Koltuniewicz, Advancement in membrane methods for liquid radioactive waste processing: current opportunities, challenges, and the global scenario, in: A.K. Pabby, S.S.H. Rizvi, A.M. Sastre (Eds.), Handbook of Membrane Separations, Chemical, Pharmaceutical, Food and Biotechnological Applications, Second edition, CRC Press Taylor & Francis Group, 2015, pp. 665–708.
- [4] A.K. Pabby, B. Swain, N.L. Sonar, V.K. Mittal, T.P. Valsala, S. Ramsubramanian, D. B. Sathe, R.B. Bhatt, S. Pradhan, Radioactive waste processing using membranes: state of the art technology, challenges and perspectives, Sep. Purif. Rev. (2021) 1–32, https://doi.org/10.1080/15422119.2021.1878221.
- [5] N. Combernoux, L. Schrive, V. Labed, Y. Wyart, E. Carretier, P. Moulin, Treatment of radioactive liquid effluents by reverse osmosis membranes: from lab-scale to pilot-scale, Water Res. 123 (2017) 311–320, https://doi.org/10.1016/j. watres.2017.06.062.
- [6] D. Chen, F. Li, X. Zhao, Y. Sun, The influence of salts on the reverse osmosis performance treating simulated boron-containing low level radioactive wastewater, J. Chem. Technol. Biotechnol. 93 (2018) 3607–3612, https://doi.org/ 10.1002/jctb.5740.
- [7] T.T.H. Dang, Ch.-W. Li, K.-H. Choo, Comparison of low-pressure reverse osmosis filtration and polyelectrolyte-enhanced ultrafiltration for the removal of Co and Sr from nuclear plant wastewater, Sep. Purif. Technol. 157 (2016) 209–214, https:// doi.org/10.1016/j.seppur.2015.11.019.
- [8] A. Miśkiewicz, G. Zakrzewska-Kołtuniewicz, Application of biosorbents in hybrid ultrafiltration/sorption processes to remove radionuclides from low-level

- radioactive waste, Desalin. Water Treat. 242 (2021) 47–55, https://doi.org/
- [9] X. Zhang, L. Niu, F. Li, X. Zhao, H. Hu, Enhanced rejection of cations by low-level cationic surfactant during ultrafiltration of low-level radioactive wastewater, Sep. Purif. Technol. 175 (2017) 314–320, https://doi.org/10.1016/j. seppur.2016.11.052.
- [10] C. Cojocaru, G. Zakrzewska-Trznadel, A. Jaworska, Removal of cobalt ions from aqueous solutions by polymer assisted ultrafiltration using experimental design approach, part 1: optimization of complexation conditions, J. Hazard. Mater. 169 (2009) 599–609, https://doi.org/10.1016/j.jhazmat.2009.03.145.
- [11] C. Cojocaru, G. Zakrzewska-Trznadel, A. Miśkiewicz, Removal of cobalt ions from aqueous solutions by polymer assisted ultrafiltration using experimental design approach, part 2: optimization of hydrodynamic conditions for a cross-flow ultrafiltration module with rotating part, J. Hazard. Mater. 169 (2009) 610–620, https://doi.org/10.1016/j.jhazmat.2009.03.148.
- [12] N. Uzal, A. Jaworska, A. Miśkiewicz, G. Zakrzewska-Trznadel, C. Cojocaru, Optimization of Co2+ ions removal from water solutions by application of soluble PVA and sulfonated PVA polymers as complexing agents, J. Colloid Interface Sci. 362 (2011) 615–624, https://doi.org/10.1016/j.jcis.2011.06.072.
- [13] A. Miśkiewicz, A. Nowak, J. Pałka, G. Zakrzewska-Kołtuniewicz, Liquid low-level radioactive waste treatment using an electrodialysis process, Membranes 11 (324) (2021) 1–12, https://doi.org/10.3390/membranes11050324.
- [14] F. Jia, Y. Yin, J. Wang, Removal of cobalt ions from simulated radioactive wastewater by vacuum membrane distillation, Prog. Nucl. Energy 103 (2018) 20–27, https://doi.org/10.1016/j.pnucene.2017.11.008.
- [15] X. Wen, F. Li, B. Jiang, X. Zhang, X. Zhao, Effect of surfactants on the treatment of radioactive laundry wastewater by direct contact membrane distillation, Chem. Technol. Biotechnol. 93 (2018) 2252–2261, https://doi.org/10.1002/jctb.5568.
- [16] G. Wu, L. Cui, Y. Xu, A novel submerged rotating membrane bioreactor and reversible membrane fouling control, Desalination 228 (2008) 255–262, https://doi.org/10.1016/j.desal.2007.10.014.
- [17] G. Zakrzewska-Trznadel, M. Harasimowicz, A. Miśkiewicz, A. Jaworska, E. Dłuska, S. Wroński, Reducing fouling and boundary-layer by application of helical flow in ultrafiltration module employed for radioactive wastes processing, Desalination 240 (2009) 108–116, https://doi.org/10.1016/j.desal.2007.10.091.
- [18] S.M. Ali, Y. Kim, A. Qamar, G. Naidu, S. Phuntsho, N. Ghaffourc, J. S. Vrouwenvelder, H.K. Shon, Dynamic feed spacer for fouling minimization in forward osmosis process, Desalination 515 (1) (2021), 115198, https://doi.org/10.1016/j.desal.2021.115198.
- [19] R. Kumar, A.F. Ismail, Fouling control on microfiltration/ultrafiltration membranes: effects of morphology, hydrophilicity, and charge, J. Appl. Polym. Sci. 42042 (2015) 1–20, https://doi.org/10.1002/app.42042.
- [20] Y. Liu, X. Li, Y. Yang, W. Ye, J. Ren, Z. Zhou, Si Ji, Analysis of the major particlesize based foulants responsible for ultrafiltration membrane fouling in polluted raw water, Desalination 347 (2014) 191–198, https://doi.org/10.1016/j. desal.2014.05.039.
- [21] K.N. Bourgeous, J.L. Darby, G. Tchobanoglous, Ultrafiltration of wastewater: effects of particles, mode of operation, and backwash effectiveness, Water Res. 35 (2001) 77–90. https://doi.org/10.1016/s0043-1354(00)00225-6.
- [22] J.C. Chen, Q. Li, M. Elimelech, In situ monitoring techniques for concentration polarization and fouling phenomena in membrane filtration, Adv. Colloid Interf. Sci. 107 (2004) 83–108, https://doi.org/10.1016/j.cis.2003.10.018.
- [23] X. Li, H. Zhang, Y. Hou, Y. Gao, J. Li, W. Guo, H.H. Ngo, In situ investigation of combined organic and colloidal fouling for nanofiltration membrane using ultrasonic time domain reflectometry, Desalination 362 (2015) 43–51, https://doi. org/10.1016/j.desal.2015.02.005.
- [24] L. Fortunato, S. Bucs, R.V. Linares, C. Calib, J.S. Vrouwenvelder, T. Leiknes, Spatially-resolved in-situ quantification of biofouling using optical coherence tomography (OCT) and 3D image analysis in a spacer filled channel, J. Membr. Sci. 524 (2017) 673–681, https://doi.org/10.1016/j.memsci.2016.11.052.
- [25] M.M. Rahman, S. Al-Sulaimi, A.M. Farooque, Characterization of new and fouled SWRO membranes by ATR/FTIR spectroscopy, Appl. Water Sci. 8 (2018) 183, https://doi.org/10.1007/s13201-018-0806-7.
- [26] A. Ruiz-García, N. Melián-Martel, V. Mena, Fouling characterization of RO membranes after 11 years of operation in a brackish water desalination plant, Desalination 430 (2018) 180–185, https://doi.org/10.1016/j.desal.2017.12.046.
- [27] N.W. Bristow, S.J. Vogt, K.T. O'Neill, J.S. Vrouwenvelder, M.L. Johns, E. O. Fridjonsson, Flow field in fouling spiral wound reverse osmosis membrane modules using MRI velocimetry, Desalination 491 (2020), 114508, https://doi.org/10.1016/j.desal.2020.114508.
- [28] H.J. Pant, Applications of the radiotracer in the industry: a review, Appl. Rad. Isot. (2021), 110076, https://doi.org/10.1016/j.apradiso.2021.110076.
- [29] R.M. Mc Donogh, H. Bauser, N. Stroh, U. Grauschopf, Experimental in situ measurement of concentration polarization during ultra- and micro-filtration of bovine serum albumin and Dextran Blue solutions, J. Membr. Sci. 104 (1995) 51–63, https://doi.org/10.1016/0376-7388(95)00011-z.
- [30] A. Miśkiewicz, G. Zakrzewska-Kołtuniewicz, The application of the radiotracer method for the investigation of the cake layer formation on the membrane surface in the cross-flow flat-sheet membrane module, Desalin. Water Treat. 128 (2018) 228–235, https://doi.org/10.5004/dwt.2018.22866.
- [31] A. Miśkiewicz, G. Zakrzewska-Trznadel, A. Dobrowolski, A. Jaworska-Sobczak, Using tracer methods and experimental design approach for examination of hydrodynamic conditions in membrane separation modules, Appl. Radiat. Isot. 70 (2012) 837–847, https://doi.org/10.1016/j.apradiso.2012.02.033.

- [32] G. Zakrzewska-Trznadel, M. Harasimowicz, Removal of radionuclides by membrane permeation combined with complexation, Desalination 144 (2002) 207–212, https://doi.org/10.1016/S0011-9164(02)00313-2.
- [33] A.G. Hassabo, A. Mendrek, C. Popescu, H. Keul, M. Möller, Deposition of functionalized polyethylenimine-dye onto cotton and wool fibres, Res. J. Text. Appar. 18 (1) (2014) 36–49, https://doi.org/10.1108/RJTA-18-01-2014-B006.
- [34] E. Salehi, S.S. Madaeni, Influence of conductive surface on adsorption behavior of ultrafiltration membrane, Appl. Surf. Sci. 256 (2010) 3010–3017, https://doi.org/ 10.1016/j.apsusc.2009.11.065.
- [35] H. Li, P. Yu, Y. Luo, Correlation between organic fouling of reverse-osmosis membranes and various interfacial interactions, Chem. Eng. Technol. 38 (1) (2015) 131–138, https://doi.org/10.1002/ceat.201400379.